J. Fluid Mech. (1992), *vol.* 238, *pp.* 487–507
Printed in Great Britain

Similarity solutions for viscous vortex cores

By ERNST W. MAYER AND KENNETH G. POWELL
Department of Aerospace Engineering, The University of Michigan, Ann Arbor, MI 48109, USA

(Received 8 June 1990 and in revised form 5 October 1991)

Results are presented for a class of self-similar solutions of the steady, axisymmetric Navier–Stokes equations, representing the flows in slender (quasi-cylindrical) vortices. Effects of vortex strength, axial gradients and compressibility are studied. The presence of viscosity is shown to couple the parameters describing the core growth rate and the external flow field, and numerical solutions show that the presence of an axial pressure gradient has a strong effect on the axial flow in the core. For the viscous compressible vortex, near-zero densities and pressures and low temperatures are seen on the vortex axis as the strength of the vortex increases. Compressibility is also shown to have a significant influence upon the distribution of vorticity in the vortex core.

1. Introduction

Vortex flows occur in nearly every area of continuum fluid mechanics – from the stirred fluid in a teacup to the flows in tornado funnels and hurricanes. An important instance of vortices in aerodynamics is the flow about a slender delta wing at angle of attack, in which the rolling up of the vortex sheets over the leading edges produces a vortex pair. These leading-edge vortices often have a roughly axisymmetric core region where viscous effects are important, and velocity and pressure gradients may be large.

Experimental studies of incompressible flows past delta wings at incidence have shown some remarkable features, including core velocities that are four to five times the free-stream values, accompanied by high gradients in the static and total pressures (Earnshaw 1961; Verhaagen & Ransbeeck 1990). Compressible flows past delta wings have shown similar velocity and pressure gradients, accompanied by near-vacuum values of density on the core axis (Monnerie & Werlé 1968).

Analytical and numerical investigations of incompressible leading-edge vortices have duplicated, at least qualitatively, many of these results. The incompressible solutions of Hall (1961), Stewartson & Hall (1963) and Powell & Murman (1988) give axial velocity and static pressure values that agree fairly well with experiment. The similarity formulations of Long (1961), Sullivan (1959) and Lewellen (1962), developed to model the flows of confined vortices, show some features which might be expected to be seen in broader physical contexts as well, although the similarity coordinates used in these studies are rather specialized and not always rigorously justified. The present work generalizes the quasi-cylindrical, or 'slender', vortex models, where variations in flow quantities are taken to occur predominantly in the radial coordinate, to include the effects of variations in the external axial flow field on the flow in the viscous core of the vortex.

Theoretical studies of compressible vortices are few in number and have given less satisfactory results. The compressible model of Brown (1965) for an inviscid

rotational flow shows compressibility to have a boundary-layer effect on the velocity field, leading to finite values of the flow quantities on the vortex axis in contrast to the inviscid incompressible case, where velocities and pressure are singular there. Mack (1960) studied a viscous heat-conducting compressible vortex, but the flow field is a rather contrived one, with density becoming unbounded at the surface of a rotating cylinder in the core which drives the flow. Hall (1966) has given qualitative arguments concerning some of the expected features of viscous compressible vortex cores, and simplified core models are important here because they lead to analytical and numerical solutions which can be more easily compared with such predictions and allow the effects of individual flow parameters to be examined in detail.

2. Solutions for incompressible vortex cores

2.1. *Governing equations*

The governing equations are the equation of conservation of mass (continuity) and the Navier–Stokes equations of conservation of momentum, expressed in cylindrical polar coordinates r, θ and z, with z taken to coincide with the vortex axis. In this study, there will be assumed to exist a value of the radial coordinate beyond which the density and axial velocity are independent of r; these 'free stream' quantities are denoted $\rho_\infty(z)$ and $W(z)$, respectively. For a steady, axisymmetric, laminar, incompressible flow the equations of motion are, in non-dimensional form,

$$\frac{1}{r}\frac{\partial}{\partial r}(ru)+\frac{\partial w}{\partial z}=0, \tag{1a}$$

$$u\frac{\partial u}{\partial r}+w\frac{\partial u}{\partial z}-\frac{v^2}{r}=-\frac{\partial p}{\partial r}+\frac{1}{Re}\left[\frac{1}{r}\frac{\partial}{\partial r}\left(r\frac{\partial u}{\partial r}\right)+\frac{\partial^2 u}{\partial z^2}-\frac{u}{r^2}\right], \tag{1b}$$

$$u\frac{\partial v}{\partial r}+w\frac{\partial v}{\partial z}+\frac{uv}{r}=\frac{1}{Re}\left[\frac{1}{r}\frac{\partial}{\partial r}\left(r\frac{\partial v}{\partial r}\right)+\frac{\partial^2 v}{\partial z^2}-\frac{v}{r^2}\right], \tag{1c}$$

$$u\frac{\partial w}{\partial r}+w\frac{\partial w}{\partial z}=-\frac{\partial p}{\partial z}+\frac{1}{Re}\left[\frac{1}{r}\frac{\partial}{\partial r}\left(r\frac{\partial w}{\partial r}\right)+\frac{\partial^2 w}{\partial z^2}\right], \tag{1d}$$

where the radial and axial coordinates r and z are non-dimensionalized with some lengthscale L; u, v and w are the radial, azimuthal and axial components of the velocity vector, respectively, non-dimensionalized with $W(1)$; ρ and p are the density and pressure, non-dimensionalized with ρ_∞ and $\rho_\infty W^2(1)$, respectively. The Reynolds number is defined as

$$Re=\frac{\rho_\infty W(1)L}{\mu}, \tag{2}$$

where μ is the viscosity of the fluid and $\rho_\infty(z)$ and $W(z)$ are evaluated at a non-dimensional axial distance of unity.

2.2. *Similarity variables*

The most practical way to simplify the above partial differential equations is to assume that flow quantities are self-similar relative to some set of coordinates. The following set of orthogonal coordinates is used in this study:

$$\phi=\frac{r}{z^n}, \quad \zeta=(nr^2+z^2)^{\frac{1}{2}}. \tag{3}$$

Here, ϕ is a 'radial' and ζ an 'axial' coordinate. The azimuthal coordinate θ remains unchanged under the transformation. For various values of n, these coordinates represent mutually orthogonal families of curves in planes $\theta =$ constant. For $n = 1$ these are rays and circles, for $n = \frac{1}{2}$ they are parabolas and ellipses and for $n = 0$ the original coordinates are recovered, i.e. $\phi = r$ and $\zeta = z$. For the present analysis, only the radial coordinate is important – the full coordinate transformation might be needed if these coordinates lent themselves to some particular geometry of interest and one wished to formulate the full equations of motion in them.

If axial derivatives are assumed to vanish in the transformed equations of motion, then the parameter n sets the rate of growth of the vortex with increasing z. If the radial extent of the viscous core is characterized by some location r_{core}, then $n = \frac{1}{2}$ and $n = 1$ correspond to parabolic ($r_{\text{core}} \propto z^{\frac{1}{2}}$) and conical ($r_{\text{core}} \propto z$) vortex growth, respectively. The $n = 0$ case represents a columnar vortex. The assumption of slenderness leads to the following rescaling for ϕ:

$$\tilde{\phi} = \phi/\epsilon, \quad 0 < \epsilon \ll 1. \tag{4}$$

The flow variables in (1) are now assumed to take the following form:

$$u(r,z) = \epsilon z^l W(z)\,\tilde{u}(\tilde{\phi}), \tag{5a}$$

$$v(r,z) = z^q W(z)\,\tilde{v}(\tilde{\phi}), \tag{5b}$$

$$w(r,z) = W(z)\,\tilde{w}(\tilde{\phi}), \tag{5c}$$

$$p(r,z) = p_\infty + z^s \rho W^2(z)\,\tilde{p}(\tilde{\phi}). \tag{5d}$$

The powers of the z in the scalings will be determined in each case by substitution into the equations of motion and requiring self-similarity to hold. For the appropriate balance of viscous and convective terms, $Re \times r_{\text{core}}^2 = O(1)$ which implies $\epsilon = (1/Re)^{\frac{1}{2}}$.

2.3. *A family of similarity solutions for viscous incompressible vortex cores*

The class of flows which will be considered is that of a slender viscous vortex in an external flow field having a power-law axial velocity. Substituting the self-similar forms of the flow variables (5) into (1) and dividing through by the coefficient of the highest-order derivative term in each results in the following set of equations:

$$\tilde{w}' + \left(\frac{W'}{W\tilde{\phi}_z}\right)\tilde{w} + \left(z^l \frac{\tilde{\phi}_r}{\tilde{\phi}_z}\right)\tilde{u}' + \left(\frac{z^l}{r\tilde{\phi}_z}\right)\tilde{u} = 0, \tag{6a}$$

$$\tilde{p}' - \left(\frac{z^{2q-s}}{r\tilde{\phi}_r}\right)\tilde{v}^2 = 0, \tag{6b}$$

$$\tilde{v}'' - \left[\left(\frac{z^l W}{\tilde{\phi}_r}\right)\tilde{u} + \left(\frac{W\tilde{\phi}_z}{\tilde{\phi}_r^2}\right)\tilde{w} - \frac{1}{r\tilde{\phi}_r} - \frac{\tilde{\phi}_{rr}}{\tilde{\phi}_r^2}\right]\tilde{v}' - \frac{1}{\tilde{\phi}_r^2}\left(\frac{qW}{z} + W'\right)\tilde{w} - \frac{1}{r\tilde{\phi}_r^2}\left(z^l W\tilde{u} + \frac{1}{r}\right)\tilde{v} = 0, \tag{6c}$$

$$\tilde{w}'' - \left[\left(\frac{z^l W}{\tilde{\phi}_r}\right)\tilde{u} + \left(\frac{W\tilde{\phi}_z}{\tilde{\phi}_r^2}\right)\tilde{w} - \frac{1}{r\tilde{\phi}_r} - \frac{\tilde{\phi}_{rr}}{\tilde{\phi}_r^2}\right]\tilde{w}' - \left(\frac{W'}{\tilde{\phi}_r^2}\right)\tilde{w}^2 - \frac{z^s}{\tilde{\phi}_r^2}\left[\left(\frac{Ws}{z} + \frac{2W'}{W}\right)\tilde{p} + W\tilde{\phi}_z\tilde{p}'\right] = 0. \tag{6d}$$

If the external axial flow is assumed to have the form

$$W(z) = w_1 z^m, \tag{7}$$

then requiring that all the coefficients in (6) be functions of $\tilde{\phi}$ only leads to the following parameter values:

$$n = \tfrac{1}{2}(1-m), \quad l = -\tfrac{1}{2}(1+m), \quad q = s = 0. \tag{8}$$

The first of these reveals the manner in which viscosity couples the parameters m and n. For the flows to be physically reasonable, the total pressure of the external flow should be taken to be a constant, denoted $(p_0)_e$; this replaces the constant p_∞ appearing in (5d). It should also be noted that the scaled radial coordinate,

$$\tilde{\phi}(r,z) = (Re)^{\frac{1}{2}} r z^{\frac{m-1}{2}} \quad (Re \text{ based on } w_1), \tag{9}$$

has the same form as the similarity coordinate of the Falkner–Skan theory for the boundary layer over a flat plate. This means that the core of a self-similar incompressible vortex in an axial pressure gradient due to an axial velocity field of the form (7) should grow like the analogous Falkner–Skan boundary layer, assuming that the pressure takes the form (5d), which implies that the static pressure coefficient is assumed to have no axial variation. The resulting equations are

$$\tilde{u}' + \frac{\tilde{u}}{\tilde{\phi}} - \tfrac{1}{2}(1-m)\,\tilde{\phi}\tilde{w}' + m\tilde{w} = 0, \tag{10a}$$

$$\tilde{p} = \frac{\tilde{v}^2}{\tilde{\phi}}, \tag{10b}$$

$$\tilde{v}'' - \left[\tilde{u} - \tfrac{1}{2}(1-m)\,\tilde{\phi}\tilde{w} - \frac{1}{\tilde{\phi}}\right]\tilde{v}' - \left[m\tilde{w} + \frac{1}{\tilde{\phi}}\left(\tilde{u} + \frac{1}{\tilde{\phi}}\right)\right]\tilde{v} = 0, \tag{10c}$$

$$\tilde{w}'' - \left[\tilde{u} - \tfrac{1}{2}(1-m)\,\tilde{\phi}\tilde{w} - \frac{1}{\tilde{\phi}}\right]\tilde{w}' + \tfrac{1}{2}(1-m)\,\tilde{v}^2 - m\tilde{w}^2 - 2m\tilde{p} = 0. \tag{10d}$$

The boundary conditions are taken to be

$$\tilde{\phi} = 0\text{:}\ \begin{cases} \tilde{u} = 0 \\ \tilde{v} = 0 \\ \tilde{w}' = 0, \end{cases} \qquad \tilde{\phi} = \tilde{\phi}_e\text{:}\ \begin{cases} \tilde{v} = \tilde{v}_e \\ \tilde{w} = 1 \\ \tilde{p} = \tilde{p}_e = -\tfrac{1}{2}(1+\tilde{v}_e^2) \end{cases} \tag{10e}$$

where $\tilde{\phi}_e$ refers to the outer edge of the computational domain. The velocity boundary conditions are much as in the inviscid case described by Hall (1961), but the viscous nature of the flow now imposes the additional requirement that the swirl velocity and the gradient of the axial velocity should both vanish on the axis. The expression for the edge pressure results from noting that

$$p_e = (p_0)_e - \tfrac{1}{2}\rho W^2(z)\,(1+\tilde{v}_e^2) \tag{11}$$

by Bernoulli's law, and solving for $\tilde{p}_e$ in (5d) results in the given dependence of scaled edge pressure on edge swirl ratio. Note that in the above, $\tilde{\phi}_e$ is formally a parameter, but the solutions rapidly approach limiting curves as $\tilde{\phi}_e$ becomes large relative to the extent of the viscous region. The solutions form a two-parameter family, depending only on the vortex strength as characterized by the swirl velocity, and m.

2.4. *The solutions for* $m = 0$

Hall (1961) considered the inviscid leading-edge vortex in a uniform external axial flow. Assuming conical self-similarity, he obtained an exact solution for the flow field in which the radial velocity varied linearly with the radial coordinate and both the swirl and axial velocities exhibited a log-like singularity on the vortex axis. This solution can be easily extended to the more general similarity variables given by (3), since the parameter n is decoupled from m in the inviscid case. An exact solution is obtainable for arbitrary n, this parameter acting only as a linear scaling in the radial velocity, the other flow variables being identical to those found by Hall.

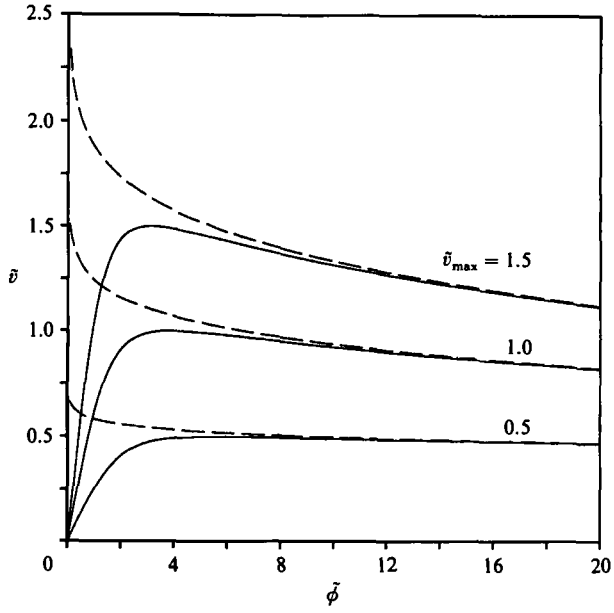

FIGURE 1. Incompressible vortex ($m = 0$): swirl velocity. ---, Inviscid; ——, viscous.

In the same paper, Hall developed a model of the viscous leading-edge vortex by matching the conical inviscid solution to a non-conical viscous inner solution. These solutions showed reasonably good agreement with the experimental data of Earnshaw (1961). Stewartson & Hall (1963) later corrected some inconsistencies in the matching procedure used in Hall (1961), the resulting solutions (to the asymptotic order given), however, appeared to be little different from those in Hall's original work.

The core model of Powell & Murman (1985) assumes steady flow, W = constant, conical self-similarity and slenderness in the viscous limit as $Re \to \infty$, reducing the Navier–Stokes equations to a system of ordinary differential equations which are then solved numerically. The results show the same features as those of Hall, and form a one-parameter family of solutions, the single parameter characterizing the solutions being the maximum swirl velocity of the vortex. In these solutions, the level of total pressure loss in the core depends only on the strength of the vortex and is independent of the Reynolds number (though the distribution of total pressure in physical variables is not) which is a desirable result, since this behaviour has also been seen in other numerical solutions of the Euler and Navier–Stokes equations for leading-edge vortex flows (Murman & Powell 1985; Powell 1989) as well as experiments (Monnerie & Werlé 1968). However, since in the previous section conical self-similarity was shown not to hold for the viscous core flow when $m = 0$, the solutions of (10) with the proper value of the core growth rate parameter, $n = \frac{1}{2}$, are now considered.

It should be noted that since only derivatives of the pressure appear in the equations in this case, the pressure coefficients will be independent of the edge pressure $\tilde{p}_e$. Also, the radial momentum equation (10*b*) in this case is decoupled from the other equations, allowing it to be integrated separately. The three coupled equations (10*a*, *c*, *d*) are rewritten as a set of five first-order equations which are linearized, discretized using a box scheme and solved numerically using a Newton iteration procedure. With a reasonable initial guess, convergence to double-precision

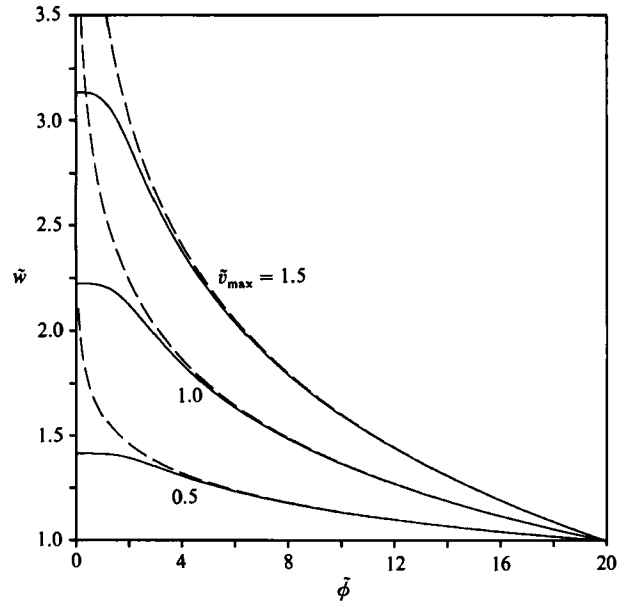

FIGURE 2. Incompressible vortex ($m = 0$): axial velocity. ---, Inviscid; ——, viscous.

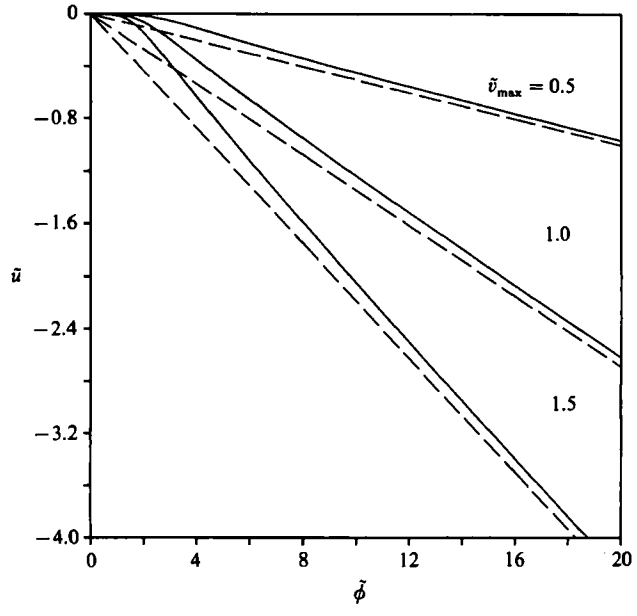

FIGURE 3. Incompressible vortex ($m = 0$): radial velocity. ---, Inviscid; ——, viscous.

machine zero typically takes only five or six iterations, on a grid fine enough to provide a mesh-converged solution. Because the maximum swirl velocity (taken to define the extent of the core) in the vortex is not known *a priori* but rather is part of the solution, the solution algorithm iterates on the edge swirl $\tilde{v}_e$ until the desired $\tilde{v}_{max}$ is reached in the converged solution.

The solutions are presented in figures 1–6. Figures 1, 2 and 3 show swirl, axial and radial velocity distributions for vortices of three different strengths. The swirl

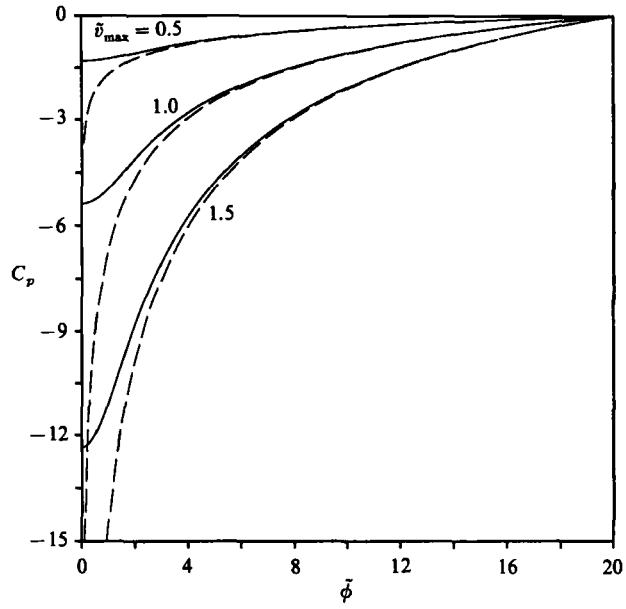

FIGURE 4. Incompressible vortex ($m = 0$): static pressure coefficient. ---, Inviscid; ——, viscous.

velocity distributions reveal a solid-body rotation near the vortex axis, with velocity reaching a maximum at a value of the scaled radial coordinate which is $O(1)$ and decaying farther out. The axial velocity profiles show a jet-like overshoot on the axis which becomes quite pronounced as the vortex strength increases. The radial velocity is everywhere non-positive, indicating fluid entrainment into the core, and is nearly linear at large distances from the axis. It is evident that all three scaled velocity components are $O(1)$ in the viscous region, as desired. The figures show that, as the strength of the vortex increases, the magnitude of the radial velocity in the core increases markedly, indicating that the rate of entrainment of fluid into the core is increasing. For comparison, the corresponding inviscid solutions (i.e. the generalization of Hall's inviscid solution to $n = \frac{1}{2}$) are plotted as dashed lines in the figures. It can be seen that outside of the core region, the solutions are essentially inviscid (it is perhaps not obvious from figure 3 that the radial velocity profile asymptotically approaches the inviscid profile, but plotting the solution at larger $\tilde{\phi}$ shows this to be the case). Figures 4 and 5 show the static and total pressure distributions, with the static pressure coefficient C_p and total pressure coefficient C_{p_0} defined as

$$C_p = \frac{p - p_e}{\frac{1}{2}\rho W^2}, \quad C_{p_0} = \frac{p_0 - p_{0e}}{\frac{1}{2}\rho W^2}. \tag{12}$$

The solutions show that the static pressure loss on the axis increases as $\tilde{v}_{max}$ increases; the total pressure loss in the core increases quadratically with $\tilde{v}_{max}$. The scaled axial component of vorticity is defined as

$$\tilde{\omega}_z = \left(\tilde{v}' + \frac{\tilde{v}}{\tilde{\phi}}\right), \tag{13}$$

and is plotted in figure 6. The vorticity is high in a narrow region near the axis and

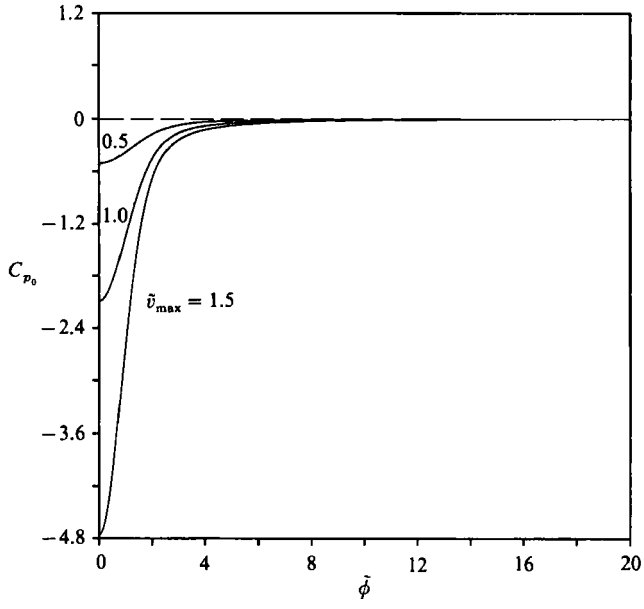

FIGURE 5. Incompressible vortex ($m = 0$): total pressure coefficient. ---, Inviscid; ——, viscous.

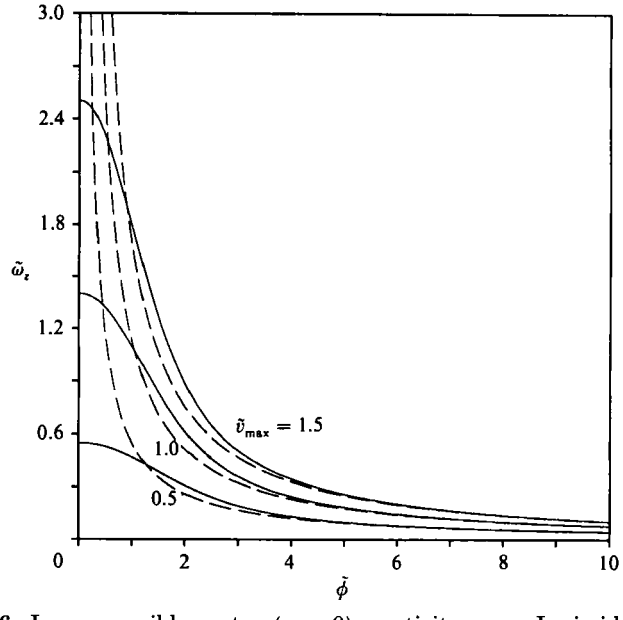

FIGURE 6. Incompressible vortex ($m = 0$): vorticity. ---, Inviscid; ——, viscous.

drops off rapidly farther out. One interesting feature seen in the vorticity plots is that the vorticity of the viscous solution is actually larger than that of the inviscid solution in a small region just away from the axis. This appears to be purely a viscous displacement effect, the viscous layer near the axis causing this region of higher vorticity to be pushed outward.

Figures 7 and 8 compare the present results to the recent experimental data of

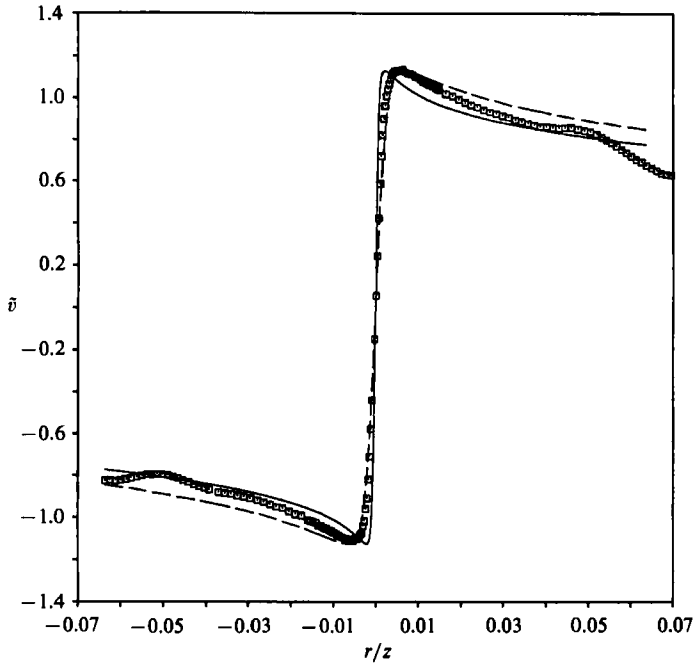

FIGURE 7. Comparison with Verhaagen & Van Ransbeeck: swirl velocity at 70% chord. ——, $\nu_e = 1$; – – –, $\nu_e = 10$; □, experiment.

Verhaagen & Van Ransbeeck (1990) who studied the leading-edge vortices produced at low Mach numbers by a large half-model delta wing at an angle of attack of 20.4°, with a free-stream Reynolds number based on root chord of 3.8×10^6. Pressure and velocity measurements were obtained using a thin 5-hole probe connected to a miniature pressure transducer. Traverses perpendicular to the wing were carried out at four axial locations along the wing – at 10, 30, 50 and 70% chord. In each figure, the experimental data at 70% chord are compared both with the theoretical profiles given by solutions of (10) with the viscosity coefficient of the laminar fluid (denoted by $\nu_e = 1$) and the solutions with an eddy viscosity ten times the free-stream viscosity (denoted $\nu_e = 10$) as an extremely simple model for the turbulence present in the experimental flows (note that (10) are unchanged if an eddy-viscosity model is used; only the Reynolds number, hence the definitions of the scaled coordinate and radial velocity change). Comparisons of swirl velocity are shown in figure 7. As can be seen, the $\nu_e = 1$ profiles give the correct qualitative behaviour, although the core diameter is underpredicted. However, the experimental data points agree extremely well with the theoretical profiles including the eddy viscosity, both in the viscous core and the inviscid outer region. Experimental and theoretical axial velocity profiles are compared in figure 8. The agreement is again very good. The axial velocities measured at the three stations further upstream, not shown here, are also in good agreement with the theoretical results. As the maximum swirl velocity was different at each chordwise station, this indicates that the coupling between the axial velocity in the core and the swirl velocity, an important feature of these flows, appears to be well described by the theory, even though the experimental flows were not truly self-similar. Comparisons of the static and total pressure coefficients given by the theory with the data from the above experiment are depicted in figures 9 and 10, respectively.

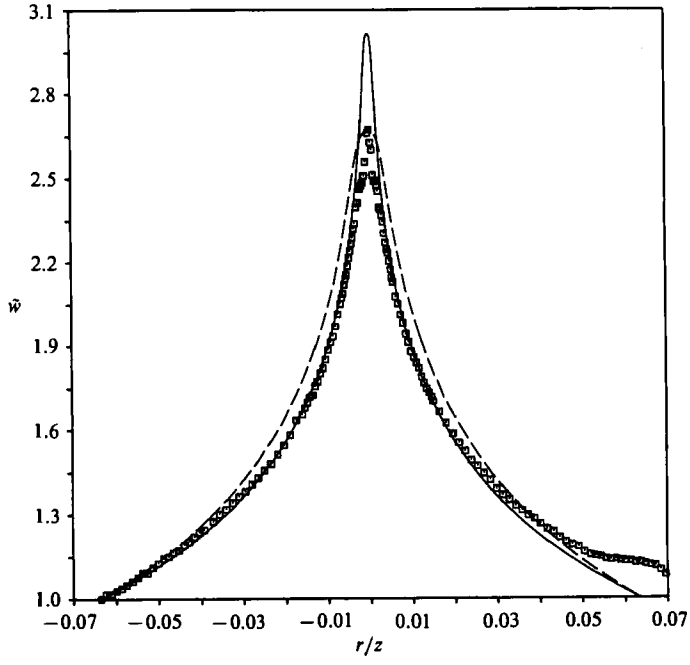

FIGURE 8. Comparison with Verhaagen & Van Ransbeeck: axial velocity at 70% chord. Legend as figure 7.

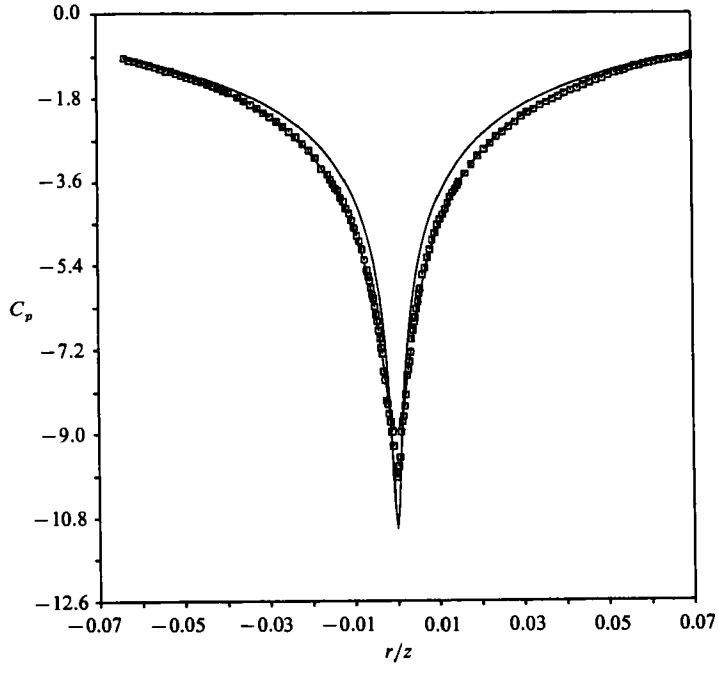

FIGURE 9. Comparison with Verhaagen & Van Ransbeeck: static pressure coefficient at 70% chord. Legend as figure 7.

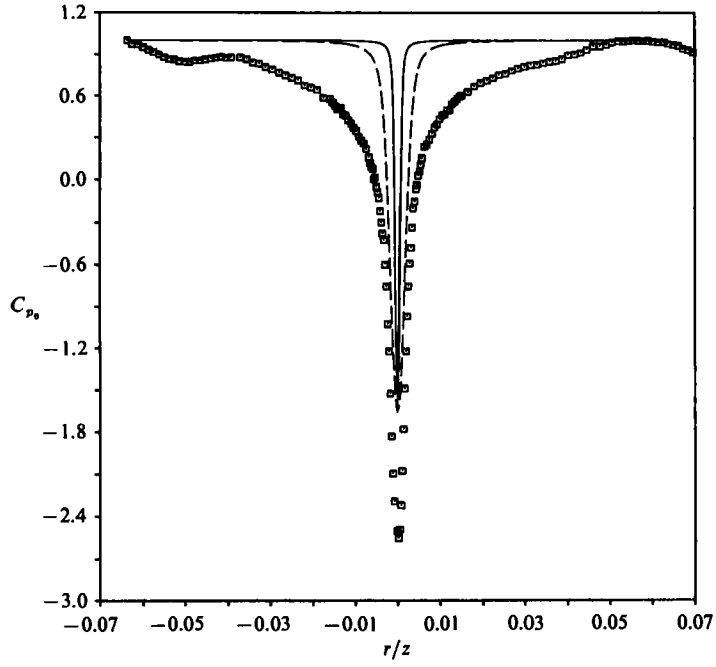

FIGURE 10. Comparison with Verhaagen & Van Ransbeeck: total pressure coefficient at 70% chord. Legend as figure 7.

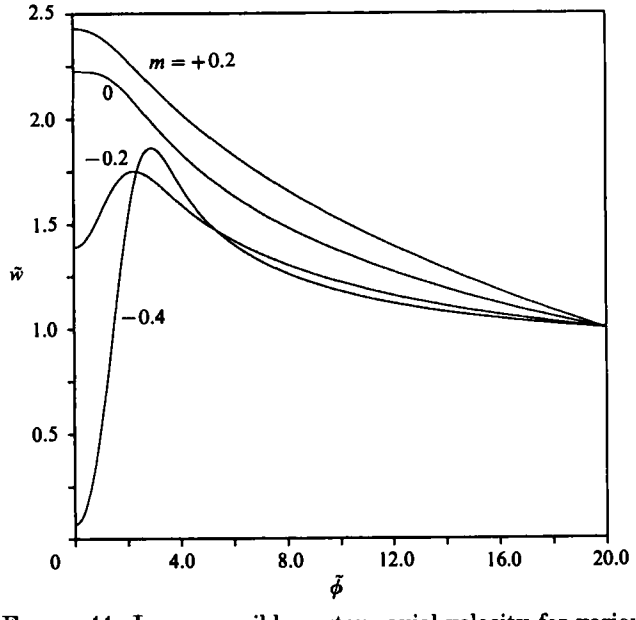

FIGURE 11. Incompressible vortex: axial velocity for various m.

2.5. *Solutions for* $m \neq 0$

The numerical solution of (10) for $m \neq 0$ is essentially the same as that described in the previous section, the main difference being that (10*b*) is no longer decoupled from the other three, resulting in a sixth-order coupled system of equations. Solutions are presented (all for flows having $\tilde{v}_{\max} = 1$) for $m = +0.2$, 0, -0.2 and -0.4,

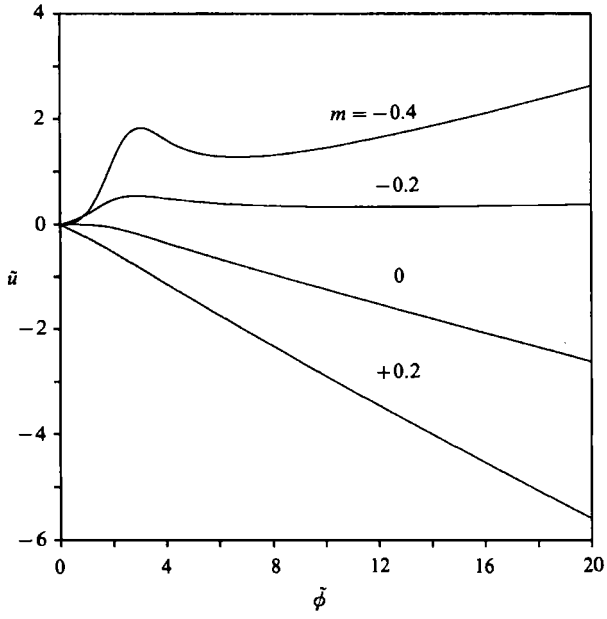

FIGURE 12. Incompressible vortex: radial velocity for various m.

corresponding to a favourable, zero and two different adverse pressure gradients. It should be noted that for external axial velocity fields with pressure gradients that are more adverse than $m = -0.2$, converged solutions were difficult to find numerically. In general, for non-zero values of m, convergence of the iteration is more difficult to achieve than for the uniform flow case, having become quite sensitive to the initial guess used in the iteration process.

The corresponding solutions exhibit some interesting features. Axial velocity profiles are depicted in figure 11. For $m > 0$, corresponding to a vortex core in a favourable axial pressure gradient, the solutions show the same qualitative features as the $m = 0$ case; however, the axial velocity peak is more localized and of greater magnitude, indicating that axial flow in the core is being accelerated.

For $m < 0$, however, the character of the solutions changes dramatically. The axial flow in the inviscid region is still in the form of a jet-like profile, but the core flow shows a pronounced retardation, eventually stagnating and actually becoming a reversed flow (with respect to the edge axial velocity) as m decreases, that is, as the pressure gradient becomes more adverse. Plots of the radial velocity $\tilde{u}$ are shown in figure 12. For favourable or zero pressure gradient, the radial velocity is negative everywhere. As m becomes more negative, i.e. as the pressure gradient becomes more adverse, the radial velocity initially shows regions of positivity near the axis and eventually becomes positive everywhere. To better understand this behaviour, it is perhaps more illuminating to consider the entrainment velocity, given by $\tilde{u} - n\tilde{\phi}\tilde{w}$, which for solutions with no reversed axial flow is everywhere non-positive, indicating that fluid crosses surfaces of constant $\tilde{\phi}$ in the inward sense.

When reversed axial flow is present in the core, the entrainment velocity is positive near the axis and changes sign further out, which corresponds to the presence of a recirculation zone in the vortex core having infinite axial extent. Qualitatively, these are similar to features seen in vortex breakdown, although the similarity formulation used obviously cannot describe behaviour with strong local axial variations such as is seen in actual breakdown structures. Finally, plots of total pressure coefficient are

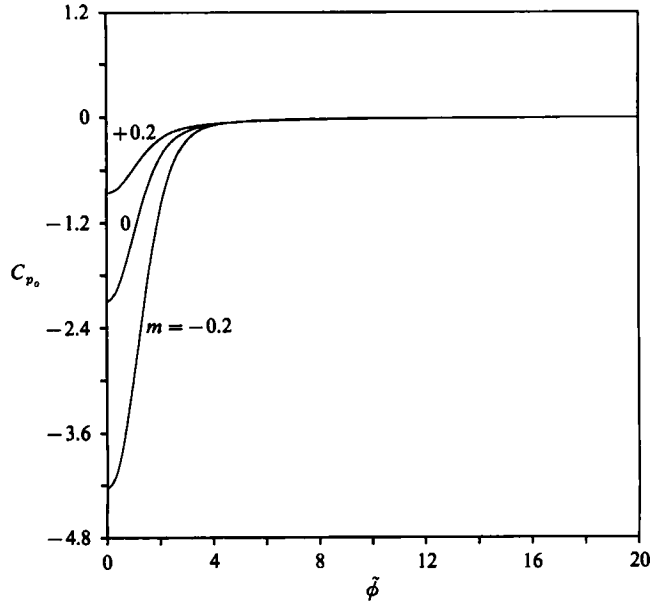

FIGURE 13. Incompressible vortex: total pressure coefficient for various m.

shown in figure 13 for $m = +0.2$, 0 and -0.2. It can be seen that the total pressure loss in the core of the vortex increases as m decreases, that is to say that as the axial pressure gradient becomes less favourable, the dissipation in the viscous core becomes greater.

3. Similarity solutions for compressible vortex cores.

Not very much theoretical work on viscous compressible vortex cores has been done to date. One main area of interest is the effect of compressibility on the flow field *vis-à-vis* the incompressible case. Hall (1966) mentions that the main effect of compressibility on the velocity field is a 'radical change in the responsiveness of the internal core structure to changes in conditions on the outside of the core', but demonstrates this only in a qualitative sense. The fact that a vortex over a given lifting surface in compressible flow may have a completely different structure than at low speeds has significant implications for slender wing configurations, where the upper-surface flow may be dominated by the vortices rolling up from the leading edge. The presence of compressibility may lead to extremely low densities and pressures in the vicinity of the axis of the vortex. Solutions to the inviscid equations of motion show that the density in the core can go to zero. Whether the presence of viscosity prevents the density from actually reaching a vacuum value is one question which solutions of the full equations of motion will address.

Another interesting phenomenon which appears in connection with compressibility is the energy separation or 'Ranque–Hilsch' effect, where the presence of viscosity in a compressible flow with curved streamlines leads, in general, to non-constant stagnation enthalpy in the flow. This is an effect not generally seen in compressible flat-plate boundary-layer theory. In the core of the viscous compressible vortex, there is a complicated balance of dissipative heating, cooling through core expansion and heat transfer between the core and the outer flow, the combination of which can lead to significant temperature gradients in the core of the vortex, as will be shown.

3.1. *Governing equations*

In cylindrical polar coordinates, the (dimensional) equations expressing conservation of mass, momentum and energy for the steady, axisymmetric flow of a viscous, heat-conducting, compressible fluid are the following, with ρ, p, T denoting density, pressure and temperature of the fluid and u, v, w denoting the radial, azimuthal and axial components of velocity vector, respectively:

$$\frac{1}{r}\frac{\partial(r\rho u)}{\partial r}+\frac{\partial(\rho w)}{\partial z}=0, \tag{14a}$$

$$\rho\left(u\frac{\partial u}{\partial r}+w\frac{\partial u}{\partial z}-\frac{v^2}{r}\right)=-\frac{\partial p}{\partial r}+\mu\left[\frac{\partial}{\partial r}\left(\frac{1}{r}\frac{\partial(ru)}{\partial r}\right)+\frac{\partial^2 u}{\partial z^2}\right]$$
$$+\frac{\mu}{3}\frac{\partial}{\partial r}\left[\frac{1}{r}\frac{\partial(ru)}{\partial r}+\frac{\partial w}{\partial z}\right]+\frac{2}{3}\frac{\partial\mu}{\partial r}\left[2\frac{\partial u}{\partial r}-\frac{u}{r}-\frac{\partial w}{\partial z}\right]+\frac{\partial\mu}{\partial z}\left(\frac{\partial w}{\partial r}+\frac{\partial u}{\partial z}\right), \tag{14b}$$

$$\rho\left(u\frac{\partial v}{\partial r}+w\frac{\partial v}{\partial z}+\frac{uv}{r}\right)=\mu\left[\frac{\partial}{\partial r}\left(\frac{1}{r}\frac{\partial(rv)}{\partial r}\right)+\frac{\partial^2 v}{\partial z^2}\right]+\frac{\partial\mu}{\partial r}\left[r\frac{\partial}{\partial r}\left(\frac{v}{r}\right)\right]+\frac{\partial\mu}{\partial z}\frac{\partial v}{\partial z}, \tag{14c}$$

$$\rho\left(u\frac{\partial w}{\partial r}+w\frac{\partial w}{\partial z}\right)=-\frac{\partial p}{\partial z}+\mu\left[\frac{1}{r}\frac{\partial}{\partial r}\left(r\frac{\partial w}{\partial r}\right)+\frac{\partial^2 w}{\partial z^2}\right]$$
$$+\frac{\partial\mu}{\partial r}\left(\frac{\partial w}{\partial r}+\frac{\partial u}{\partial z}\right)-\frac{2}{3}\frac{\partial\mu}{\partial z}\left[\frac{1}{r}\frac{\partial(ru)}{\partial r}-2\frac{\partial w}{\partial z}\right], \tag{14d}$$

$$\rho C_p\left(u\frac{\partial T}{\partial r}+w\frac{\partial T}{\partial z}\right)+\frac{T}{\rho}\left(\frac{\partial\rho}{\partial T}\bigg|_p\right)\left(u\frac{\partial p}{\partial r}+w\frac{\partial p}{\partial z}\right)$$
$$=\lambda\left[\frac{1}{r}\frac{\partial}{\partial r}\left(r\frac{\partial T}{\partial r}\right)+\frac{\partial^2 T}{\partial z^2}\right]+\frac{\partial\lambda}{\partial r}\frac{\partial T}{\partial r}+\frac{\partial\lambda}{\partial z}\frac{\partial T}{\partial z}+\mu\left\{2\left[\left(\frac{\partial u}{\partial r}\right)^2+\left(\frac{u}{r}\right)^2+\left(\frac{\partial w}{\partial z}\right)^2\right]\right.$$
$$\left.+\left[r\frac{\partial}{\partial r}\left(\frac{v}{r}\right)\right]^2+\left(\frac{\partial w}{\partial r}+\frac{\partial u}{\partial z}\right)^2+\left(\frac{\partial v}{\partial z}\right)^2-\frac{2}{3}\left[\frac{1}{r}\frac{\partial(ru)}{\partial r}+\frac{\partial w}{\partial z}\right]^2\right\}. \tag{14e}$$

Here, μ, C_p and λ are the viscosity, specific heat at constant pressure and thermal conductivity of the fluid. If μ, C_p and λ are specified as functions of the flow variables then the perfect-gas law $p \propto \rho T$ closes the equations. In the case of isentropic flow the gas is usually assumed to satisfy a polytropic relation $p \propto \rho^\gamma$, where γ is the ratio of specific heats of the gas. This results in the simple expression $c^2 = \gamma p \rho^{-1}$ for the sound speed c. The viscosity μ is generally a function of temperature which can be accurately modelled using Sutherland's law or, more simply, a power-law relation; in many cases the Prandtl number $Pr = \mu C_p \lambda^{-1}$ (a non-dimensional combination of the transport coefficients of the fluid) can be assumed to be a constant which is $O(1)$ for most gases.

3.2. *Similarity formulation and solutions for the viscous compressible vortex*

Following the inviscid solutions of Hall for incompressible vortices, Brown (1965) presented inviscid solutions for a rotational, conically self-similar compressible vortex core. The flow was taken to be both isentropic and isenthalpic. Under these assumptions, the governing equations can be reduced to a single ordinary differential equation having the fluid density as the unknown and the axial velocity as the independent coordinate, along with an auxiliary equation relating these two

quantities to the physical coordinate. As was the case with the inviscid incompressible solutions of Hall, the generalization of this formulation to arbitrary power-law self-similarity is straightforward in the case of uniform external axial flow. The resulting equations are essentially the same as those originally derived by Brown, the only difference being the appearance of the growth rate parameter n, which again acts as a linear scaling for the radial velocity. Solutions of the equations show compressibility to have a regularizing effect on the flow, the axis swirl velocity now being zero for non-zero Mach number and the axial velocity reaching the limiting value associated with fully expanded flow there, density going to zero as the axis is reached. However, derivatives of swirl and axial velocity are unbounded on the axis, behaviour which is impossible in the presence of viscosity.

To understand how a real compressible vortex behaves it is necessary to include the effects of viscosity and heat transfer. Following the analysis for the incompressible case, the similarity forms (5) for the velocities are taken, as well as the following for the density ρ and static temperature T:

$$\rho(r,z) = \rho_e(z)\,\tilde{\rho}(\tilde{\phi}), \tag{15a}$$

$$T(r,z) = T_e(z)\,(\gamma-1)M_e^2\,\tilde{T}(\tilde{\phi}), \tag{15b}$$

where the Mach number M_e is based on the edge axial velocity W and the sound speed there. The external density and temperature fields $\rho_e(z)$ and $T_e(z)$ are related to the external axial pressure field through the perfect-gas and polytropic relations. These forms are substituted into the steady, axisymmetric equations of motion (14) and the viscous limit as $Re \to \infty$ taken. Constant specific heats and Prandtl number are assumed; this is equivalent to assuming that the viscosity and thermal conductivity have the same temperature dependence. Collecting lowest-order terms in the Reynolds number, the following eighth-order system of ordinary differential equations for the three velocity components, density and temperature is obtained in the case of uniform external flow:

$$(\tilde{\rho}\tilde{u})' + \frac{\tilde{\rho}\tilde{u}}{\tilde{\phi}} - n\tilde{\phi}(\tilde{\rho}\tilde{w})' = 0, \tag{16a}$$

$$\frac{\gamma-1}{\gamma}(\tilde{\rho}\tilde{T})' = \frac{\tilde{\rho}\tilde{v}^2}{\tilde{\phi}}, \tag{16b}$$

$$\tilde{\rho}\left[(\tilde{u}-n\tilde{\phi}\tilde{w})\,\tilde{v}' + \frac{\tilde{u}\tilde{v}}{\tilde{\phi}}\right] = \tilde{\mu}\left(\tilde{v}'' + \frac{\tilde{v}'}{\tilde{\phi}} - \frac{\tilde{v}}{\tilde{\phi}^2}\right) + \tilde{\mu}'\left(\tilde{v}' - \frac{\tilde{v}}{\tilde{\phi}}\right), \tag{16c}$$

$$\tilde{\rho}[(\tilde{u}-n\tilde{\phi}\tilde{w})\,\tilde{w}' - n\tilde{v}^2] = \tilde{\mu}\left(\tilde{w}'' + \frac{\tilde{w}'}{\tilde{\phi}}\right) + \tilde{\mu}'\tilde{w}', \tag{16d}$$

$$\tilde{\rho}(\tilde{u}-n\tilde{\phi}\tilde{w})\left(\tilde{T}' - \frac{\tilde{v}^2}{\tilde{\phi}}\right) = \frac{\tilde{\mu}}{Pr}\left(\tilde{T}'' + \frac{\tilde{T}'}{\tilde{\phi}}\right) + \frac{\tilde{\mu}'\tilde{T}'}{Pr} + \tilde{\mu}\left[\left(\tilde{v}' - \frac{\tilde{v}}{\tilde{\phi}}\right)^2 + (\tilde{w}')^2\right]. \tag{16e}$$

The five boundary conditions on the velocities are the same as in the incompressible case, and are supplemented by the following conditions on the density and temperature:

$$\tilde{T}'(0) = 0, \quad \tilde{\rho}(\tilde{\phi}_e) = 1, \quad \tilde{T}(\tilde{\phi}_e) = 1/[(\gamma-1)M_e^2]. \tag{16f}$$

If the viscosity is assumed to have a power-law variation with temperature, i.e. $\tilde{\mu} = (T/T_e)^\sigma$ (where T in this relation can be either the scaled or unscaled temperature), then the only parameters in these equations are the Prandtl number

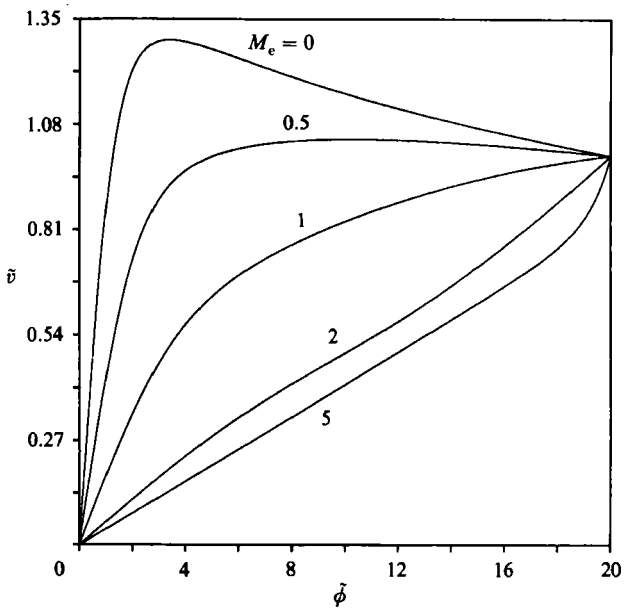

FIGURE 14. Viscous compressible vortex: swirl velocity ($\tilde{v}_e = 1$).

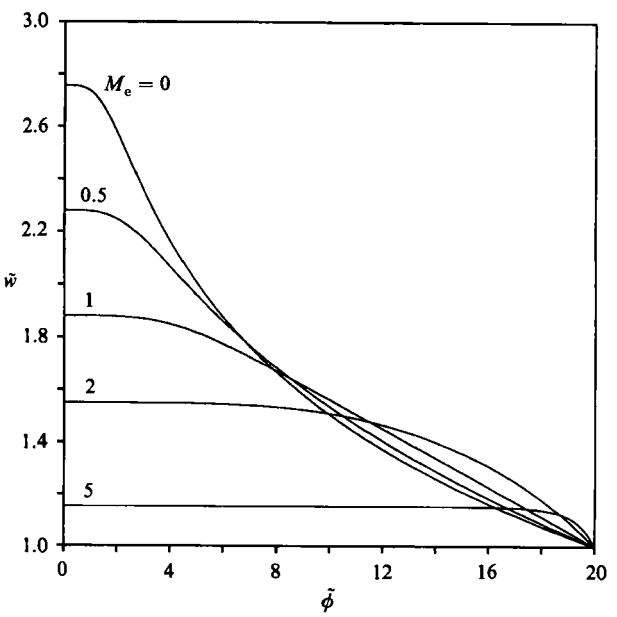

FIGURE 15. Viscous compressible vortex: axial velocity ($\tilde{v}_e = 1$).

Pr, the axial Mach number at the outer boundary M_e, the viscosity-law exponent σ and the swirl velocity at the outer boundary, which determines the strength of the vortex.

The equations are discretized and solved numerically as described in §4. Results for $m = 0$, $n = \frac{1}{2}$ and $Pr = 0.72$ (air) and constant viscosity are presented in figures 14–20, all for an edge swirl velocity $\tilde{v}_e = 1$. Figures 14, 15 and 16 show swirl, axial and radial velocity distributions for various Mach numbers. At low Mach numbers,

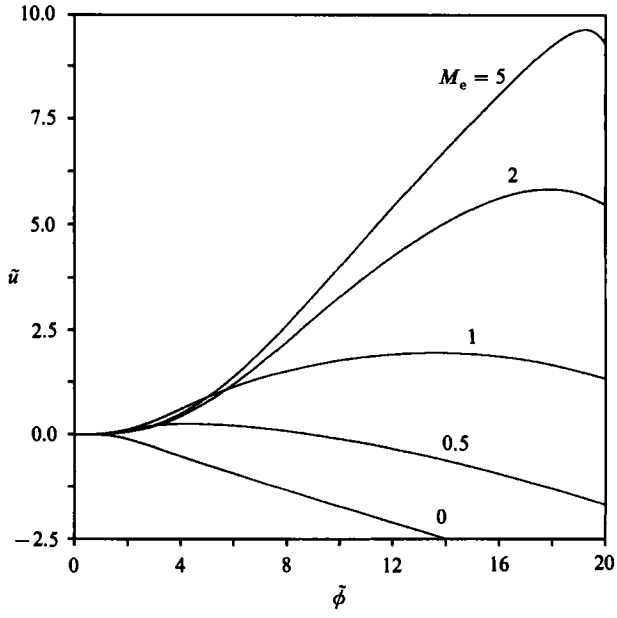

FIGURE 16. Viscous compressible vortex: radial velocity ($\tilde{v}_e = 1$).

the velocity plots look like those for the incompressible vortex. As the Mach number rises, the slope of the swirl velocity at the outer boundary decreases and then changes sign; the slope of the swirl velocity near the axis also decreases, indicating that the fluid in the core has a weaker rotation than in the incompressible case. The axial velocity peak in the core region becomes less pronounced as the Mach number rises; at high Mach numbers the axial velocity profile appears very flattened out, the peak near the axis seen at low Mach numbers having completely disappeared. Note that at the higher Mach numbers, the axial velocity rises very quickly to its maximum value near the outer boundary, but no longer reaches the limiting velocity as it did in the inviscid case. At the higher Mach numbers the core wants to expand and fill up all of space, but is constrained from doing so by the outer boundary conditions. This behaviour is also seen in solutions of the inviscid equations as the Mach number increases, and makes a smooth match to an outer flow seem unlikely, if not impossible. While the current study sheds little light on this matching problem, the solutions should be representative of flows where the vorticity is introduced at a finite distance from the vortex axis, as is the case in leading-edge flows.

The radial velocity $\tilde{u}$ is negative everywhere at very low Mach numbers, as it was in the incompressible case. As M_e rises from zero, the radial velocity becomes positive in a region near the axis which expands outward as M_e increases further, behaviour similar to that seen in the inviscid case. Figure 17 shows the static pressure coefficient distributions. As was seen in the inviscid case, the static pressure coefficient profiles become flattened out at higher Mach numbers and the magnitude of the drop in C_p at the axis is reduced as the Mach number increases. It should be noted that this does not mean that the pressure drop in the core of the compressible vortex is actually less than that of the incompressible case – the pressure coefficient is simply normalized with $\rho_e W^2$, which is also increasing as M_e increases. The distribution of C_p, however, is much less localized in the core at higher Mach numbers than in the incompressible case.

Figures 18 and 19 show distributions of density and temperature in the core. The

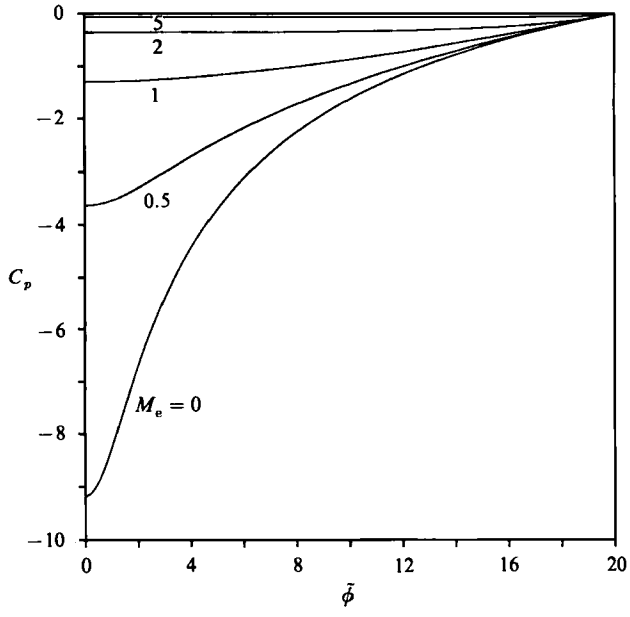

FIGURE 17. Viscous compressible vortex: static pressure coefficient ($\tilde{v}_e = 1$).

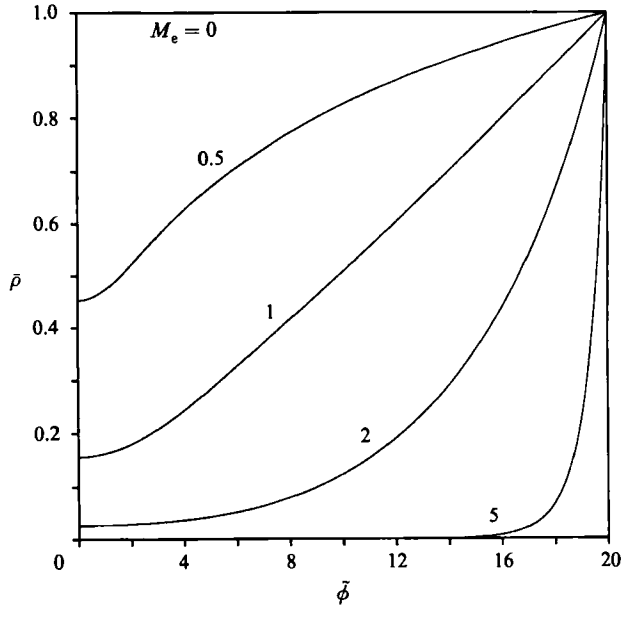

FIGURE 18. Viscous compressible vortex: density ($\tilde{v}_e = 1$).

density reaches a minimum on the axis, but viscous effects always prevent a vacuum region, although for some of the cases studied, the axis density was less than one-thousandth of the free-stream density. The temperature decreases monotonically from the outer boundary to the axis for Mach numbers that are $O(1)$, and the magnitude of the temperature drop for a given vortex strength increases as the Mach number rises. This dissipation induced by the large velocity gradients at the outer boundary makes the results somewhat suspect for larger Mach numbers – in the $M_e = 5$ case (not plotted) the temperature actually rises slightly near the outer

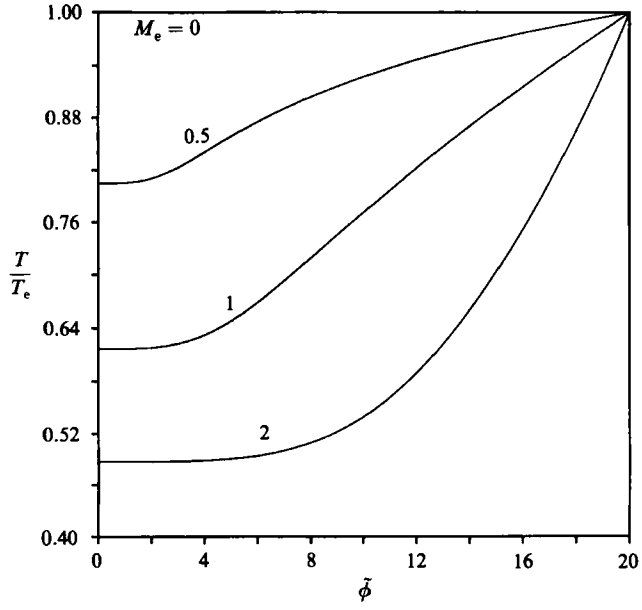

FIGURE 19. Viscous compressible vortex: temperature ($\tilde{v}_e = 1$).

boundary before reaching an axis value only slightly lower than unity. At a given M_e. the axis temperature drops as the swirl velocity increases from zero, but in all cases studied remains bounded away from zero. The achievable temperature minimum for a given M_e was found to be near zero for low Mach numbers, although the swirl velocities required to achieve this are high enough to make an experimental simulation of such a flow doubtful. At higher values of M_e, the achievable axis temperatures are not so low, but they occur at reasonable values of the edge swirl ratio, values on the order of unity, hence one would expect to see effects of these low temperatures in real flows. Visible evidence of low core temperatures can easily be seen in the water vapour which condenses in the cores of leading-edge or strake vortices shed at high angles of attack by fighter aircraft, for instance.

Another interesting result is the effect of compressibility on the vorticity distribution in the core, shown in figure 20. For the incompressible vortex there exists a concentrated core of high vorticity near the axis. It can be seen from the solutions of the compressible equations that, as the Mach number increases, this vorticity peak becomes less pronounced and, at $M_e = 2$, has completely disappeared. This indicates that for the compressible vortex, the core, as defined by its increased vorticity, may be ill-defined or disappear altogether.

Distributions of axial Mach number, not plotted here, look much like the plots of axial velocity; one difference is that while the peak value of axial velocity decreases as M_e becomes larger, the peak axial Mach number ratio M_{axis}/M_e increases monotonically. The solutions also show that the total Mach number has a maximum away from the axis, indicating that, unlike in the inviscid case, the compressibility of the flow is greatest at non-zero values of the radial coordinate in the viscous case.

The effects of varying the Prandtl number and the viscosity law were also investigated, and show that at a given edge swirl velocity and Mach number, the core temperature decreases as the Prandtl number is increased. This is because an increase in Prandtl number implies either a higher viscosity, which enhances the energy separation effect, or a lower thermal conductivity, which means less heat transfer into the cooler core. Either leads to a lower axis temperature. It was also found that

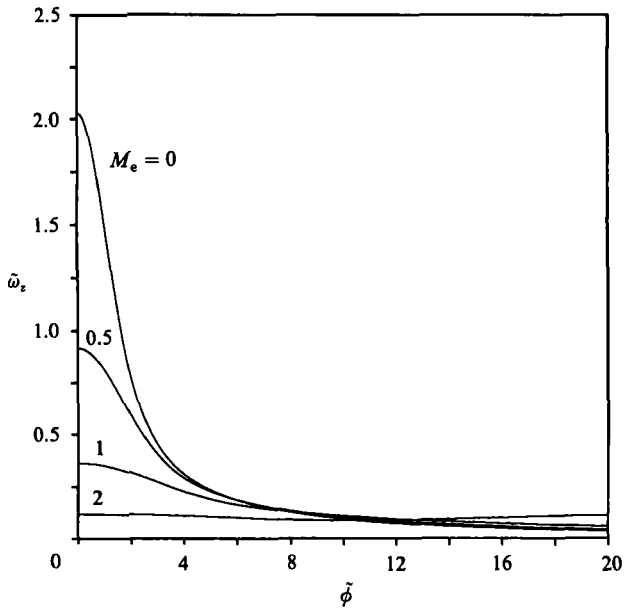

FIGURE 20. Viscous compressible vortex: vorticity ($\tilde{v}_e = 1$).

as the viscosity-law exponent σ increases from zero, the core velocities become higher and the axis density decreases more rapidly with increasing $\tilde{v}_e$, apparently because as the axis is approached, the viscosity is dropping as the temperature drops.

The above solutions show that the energy-separation effect can be quite pronounced – for free-stream axial Mach numbers of order one, the static temperature on the axis can reach values less than one-half the free-stream temperature for edge swirl angles on the order of 45°.

4. Conclusions

The approach developed in this paper leads to sets of ordinary differential equations describing a variety of axisymmetric self-similar vortical flows. This gives a reasonably unified framework in which to study the effects of flow parameters such as vortex strength, external axial pressure gradients and compressibility.

The effects of Reynolds number and edge swirl angle on the velocity and pressure distributions through the vortex core have been well-documented elsewhere. The Reynolds number acts primarily to scale the extent of the core; the edge swirl angle sets the 'strength' of the vortex, determining the magnitude of the axial velocity maximum and the static pressure minimum on the axis of the core.

The effects of external axial pressure gradient and compressibility had not been adequately studied to date. The pressure gradient primarily affects the axial flow in the core, with favourable pressure gradients accelerating the core flow, and adverse pressure gradients retarding it, even to the point of stagnation or reversal of the flow on the axis. This behaviour is qualitatively similar to that seen immediately upstream of a vortex breakdown. It seems plausible that, although the similarity assumption is restrictive in the sense that local axial variations in the flow field are excluded, and the slenderness assumption cannot be expected to hold in a region where vortex breakdown has occurred, the solutions with $m < 0$ may give a reasonable idea of what happens locally immediately upstream of the breakdown. The parameter m, describing the axial variation of the external flow, is also shown

in the presence of viscosity to be linked to the parameter n, governing the rate of growth of the viscous region, through the simple relation $m = 1-2n$. For both incompressible and compressible inviscid flow, the rate-of-growth parameter n acts only to scale the radial velocity, effectively reducing the number of parameters by one.

Compressibility has a regularizing effect on the solutions, an immediate result being that the velocities remain bounded, although their derivatives can be infinite in inviscid flow. The presence of viscosity, besides making gradients of all flow variables bounded and enforcing the condition of zero swirl on the axis, appears to prevent the creation of a vacuum in the core, although very low axis densities occur at high values of the swirl intensity. In spite of the viscous dissipation in such flows, low core temperatures can be achieved even for vortices of moderate strength.

In addition to providing insight about swirling flows in general, similarity formulations such as the ones presented, where the number of parameters is kept to a minimum, may also serve to provide useful comparison cases for large-scale numerical analyses, as well as a starting point for more general theoretical studies of the stability of swirling flows than have been advanced at present.

The authors would like to thank Earll Murman (MIT) for helpful discussions regarding the theoretical approach used in this paper. They would also like to thank Nick Verhaagen (TU Delft) for supplying experimental data for use in the comparisons, and Arthur F. Messiter (Michigan) for reading parts of the manuscript and making valuable suggestions. This work was funded by the National Science Foundation (Grant EET-8857500) and by a Research Partnership Award from the Horace H. Rackham School of Graduate Studies, the University of Michigan.

REFERENCES

BROWN, S. N. 1965 The compressible inviscid leading-edge vortex. *J. Fluid Mech.* **22**, 17–32.

EARNSHAW, P. B. 1961 An experimental investigation of the structure of a leading-edge vortex. *Aeronaut. Res. Counc. R & M* 3281.

HALL, M. G. 1961 A theory for the core of a leading-edge vortex. *J. Fluid Mech.* **11**, 209–228.

HALL, M. G. 1966 The structure of concentrated vortex cores. *Prog. Aeronaut. Sci.* **7**, 53–110.

LEWELLEN, W. S. 1962 A solution for three-dimensional vortex flows with strong circulation. *J. Fluid Mech.* **14**, 420–432.

LONG, R. R. 1961 A vortex in an infinite viscous fluid. *J. Fluid Mech.* **11**, 611–624.

MACK, L. M. 1960 The compressible viscous heat-conducting vortex. *J. Fluid Mech.* **8**, 284–292.

MONNERIE, B. & WERLÉ, H. 1968 Étude de l'Écoulement supersonique et hypersonique autour d'une aile Élancée en incidence. In *AGARD-CP*-30. pp. 23-1–23-19.

MURMAN, E. M. & POWELL, K. G. 1985 Comparison of measured and computed pitot pressures in a leading-edge vortex from a delta wing. In *Studies of Vortex-Dominated Flows*, pp. 270–281. Springer.

POWELL, K. G. 1989 *Vortical Solutions of the Conical Euler Equations.* Vieweg.

POWELL, K. G. & MURMAN, E. M. 1988 A model for the core of a slender viscous vortex. *AIAA Paper* 88-0503.

STEWARTSON, K. & HALL, M. G. 1963 The inner viscous solution for the core of a leading-edge vortex. *J. Fluid Mech.* **15**, 306–318.

SULLIVAN, R. D. 1959 A two-cell vortex solution of the Navier–Stokes equations. *J. Aerospace Sci.* **19**, 31–34.

VERHAAGEN, N. G. & VAN RANSBEECK, P. 1990 Experimental and numerical investigation of the flow in the core of a leading edge vortex. *AIAA Paper* 90-0384.